ECCOMAS Congress 2016
VII European Congress on Computational Methods in Applied Sciences and Engineering
M. Papadrakakis, V. Papadopoulos, G. Stefanou, V. Plevris (eds.)
Crete Island, Greece, 5–10 June 2016

3D BEAM-COLUMN FINITE ELEMENT UNDER NON-UNIFORM SHEAR STRESS DISTRIBUTION DUE TO SHEAR AND TORSION

Paolo Di Re[1], Daniela Addessi[1] and Filip C. Filippou[2]

[1]Department of Structural and Geotechnical Engineering, University of Rome, Sapienza
via Eudossiana 18, Rome, 00184, Italy
e-mail: {paolo.dire,daniela.addessi}@uniroma1.it

[2] Department of Civil and Environmental Engineering, University of California, Berkeley
731 Davis Hall, Berkeley, CA, United States
e-mail: filippou@berkeley.edu

Keywords: Fiber section models, Mixed Formulation, Warping, Shear and torsion, Damage.

Abstract. *The paper discusses the application of a 2-node, three-dimensional (3D) beam-column finite element with an enhanced fiber cross-section model to the inelastic response analysis of concrete members. The element accounts for the local distribution of strains and stresses under the coupling of axial, flexural, shear, and torsional effects with an enriched kinematic description that accounts for the out-of-plane deformations of the cross-section. To this end the warping displacements are interpolated with the addition of a variable number of local degrees of freedom. The material response is governed by a 3D nonlinear stress-strain relation with damage that describes the degrading mechanisms of typical engineering materials under the coupling of normal and shear stresses. The element formulation is validated by comparing the numerical results with measured data from the response of two prismatic concrete beams under torsional loading and with standard beam formulations.*

1 INTRODUCTION

Beam-column finite elements are widely used for describing the inelastic response of structural members in large scale simulations, because of the optimal balance between accuracy and computational efficiency they offer.

Among the different beam finite element models *force-based* and *mixed* formulations [1, 2, 3, 4] have proven superior to the classical *displacement-based* models under large inelastic, cyclic deformations, even with the slight increase in computational cost for the element state determination. In this framework, many researchers focused their efforts on the development of an efficient, discrete *fiber cross-section model* [5, 6] for effectively capturing the multi-axial coupling of the beam stress resultants under general constitutive material relations. While classical Euler-Bernoulli beam formulations assume that plane sections remain plane and normal to the axis and are unable to capture the effect of shear and torsion, recent studies have proposed enhanced models that account for these effects [7, 8, 9, 10]. Nonetheless, no existing model appears to give a complete and realistic representation of the cross-section warping with the resulting shear stresses and strains. According to [11] existing models fail to reproduce accurately the interaction of the shear and normal stresses along the beam axis, the local response near the boundaries, and the shear lag phenomenon.

This paper extends the 2-node 3D beam-column finite element (FE) in [12] to reinforced concrete beams. The formulation by LeCorvec is based on a modified Hu-Washizu variational potential that leads to the definition of a four-field mixed formulation. With respect to the standard Hu-Washizu mixed formulation with only three independent fields, LeCorvec's formulation introduces as fourth additional field the out-of-plane displacements due to warping of the element cross-section [12]. These displacements are interpolated at two independent levels: along the axis and over the cross-section. The degrees of freedom associated with the resulting interpolation functions constitute additional independent variables of the element allowing it to capture the evolution of the warping displacements during the loading process, and the coupling between the shear and torsion with the normal stress components.

To correctly reproduce the nonlinear behavior of the cross-section, a fiber discretization is introduced. Hence, stress and strain variables are determined at each discrete fiber and then integrated over the area to obtain the generalized section quantities. To describe the damaging mechanisms typical of brittle-like engineering materials, the isotropic 3D damage model in [15] is adopted. This considers the non-symmetric response, in tension and compression, and the unilateral effect, observed during cyclic load patterns for this material type.

The proposed FE is validated by comparing the numerical results of plain concrete (PC) and reinforced concrete (RC) beams under end torque with experimental measurements and by confronting these results with those of standard FE beam models.

2 FINITE ELEMENT FORMULATION

This section summarizes the salient features of the 3D beam-column FE formulation in [12] with the description of the warping displacements for the cross section under inelastic nonlinear material response.

The FE element formulation is based on the assumption of small end node displacements and small strains, because nonlinear geometry effects are accounted for with the corotational formulation during the transformation of the nodal response variables.

Figure 1 shows the global FE reference system (O, X, Y, Z) together with the nodal displacement vector components. These are the twelve degrees of freedom (DOFs) of a standard 3D

beam-column element, that is three translations (listed in the vectors $\mathbf{u}_{I/J}$) and three rotations (listed in the vectors $\boldsymbol{\theta}_{I/J}$) at each node:

$$\mathbf{u} = \left\{\mathbf{u}_I^T \;\; \boldsymbol{\theta}_I^T \;\; \mathbf{u}_J^T \;\; \boldsymbol{\theta}_J^T\right\}^T \tag{1}$$

The corresponding nodal force components are collected in the vector:

$$\mathbf{p} = \left\{\mathbf{p}_I^T \;\; \mathbf{m}_I^T \;\; \mathbf{p}_J^T \;\; \mathbf{m}_J^T\right\}^T \tag{2}$$

with $\mathbf{p}_{I/J}$ and $\mathbf{m}_{I/J}$ being the force and moment vectors at node I/J.

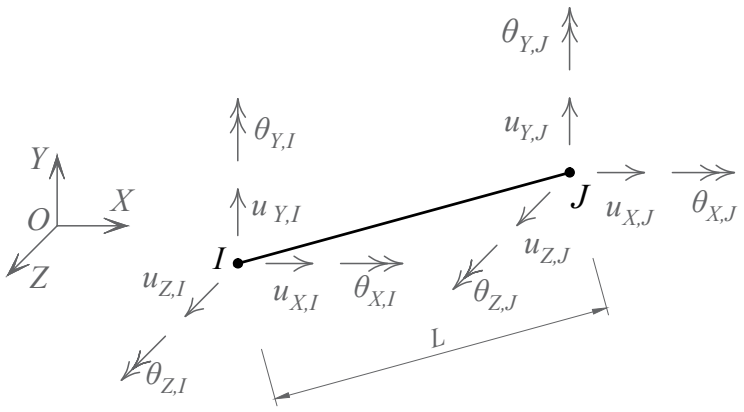

Figure 1: Global FE reference system (undeformed configuration): nodal traslation and rotation components.

By restraining the rigid body motions of the element, the basic reference system (I, x, y, z) is introduced (Figure 2), with x parallel to the axis directed from node I to node J and y and z lying in the plane of the element cross-section. Hence, the basic displacement vector $\mathbf{v}$, also called the element deformation vector, can be defined:

$$\mathbf{v} = \{u_{x,J} \quad \theta_{z,I} \quad \theta_{z,J} \quad \theta_{x,J} \quad \theta_{y,I} \quad \theta_{y,J}\}^T \tag{3}$$

where $u_{x,J}$ is the translation of node J parallel to the local axis x, $\theta_{z,I/J}$ and $\theta_{y,I/J}$ are the rotations at node I/J about the z and y–axis, respectively, and $\theta_{x,J}$ is the rotation at node J about the x–axis. The basic displacement vector $\mathbf{v}$ is obtained from the global vector $\mathbf{u}$ according to:

$$\mathbf{v} = \mathbf{a}_g\,\mathbf{u} \quad with \quad \mathbf{a}_g = \begin{bmatrix} -1 & 0 & 0 & 0 & 0 & 0 & 1 & 0 & 0 & 0 & 0 & 0 \\ 0 & 1/L & 0 & 0 & 0 & 1 & 0 & -1/L & 0 & 0 & 0 & 0 \\ 0 & 1/L & 0 & 0 & 0 & 0 & 0 & -1/L & 0 & 0 & 0 & 1 \\ 0 & 0 & 0 & -1 & 0 & 0 & 0 & 0 & 0 & 1 & 0 & 0 \\ 0 & 0 & -1/L & 0 & 1 & 0 & 0 & 0 & 1/L & 0 & 0 & 0 \\ 0 & 0 & -1/L & 0 & 0 & 0 & 0 & 0 & 1/L & 0 & 1 & 0 \end{bmatrix} \tag{4}$$

where $\mathbf{a}_g$ is the kinematic matrix and L is the undeformed element length. The basic force vector $\mathbf{q}$, corresponding to the deformation vector $\mathbf{v}$, is defined as:

$$\mathbf{q} = \{p_{x,J} \quad m_{z,I} \quad m_{z,J} \quad m_{x,J} \quad m_{y,I} \quad m_{y,J}\}^T \tag{5}$$

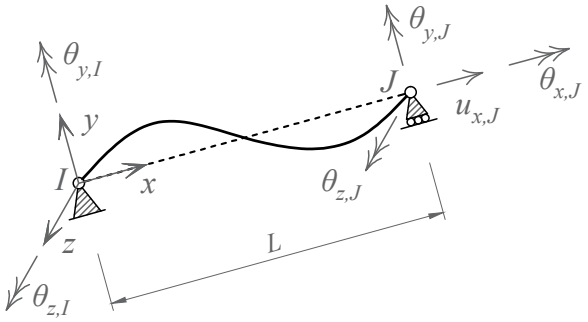

Figure 2: Basic FE reference system (deformed configuration): basic displacement components.

where $p_{x,J}$ is the force at node J in the direction of the local x–axis, $m_{z,I/J}$ and $m_{y,I/J}$ are the moments at node I/J about the z and y–axis, respectively, and $m_{x,J}$ is the moment at node J about the x–axis.

Because of the virtual work equivalence, the element stiffness matrix $\hat{\mathbf{k}}$ and the element force vector $\mathbf{p}$ in the global system can be defined through the transpose of the matrix $\mathbf{a}_g$, [2]:

$$\hat{\mathbf{k}} = \mathbf{a}_g^T \, \mathbf{f}^{-1} \, \mathbf{a}_g \qquad \text{and} \qquad \mathbf{p} = \mathbf{a}_g^T \, \mathbf{q} \tag{6}$$

where $\mathbf{f}$ is the element basic flexibility matrix, whose derivation is discussed next.

Under the assumption of the cross-section remaining rigid in plane and out of plane, the generalized section displacement vector $\mathbf{u}_s(x)$ is defined in the basic coordinate system as:

$$\mathbf{u}_s(x) = \{u(x) \quad \theta_z(x) \quad v(x) \quad \theta_x(x) \quad \theta_y(x) \quad w(x)\}^T \tag{7}$$

where $u(x)$, $v(x)$ and $w(x)$ are the translation components of the beam axis, and $\theta_x(x)$, $\theta_y(x)$ and $\theta_z(x)$ are the rotations of the cross-section (Figure 3(a)).

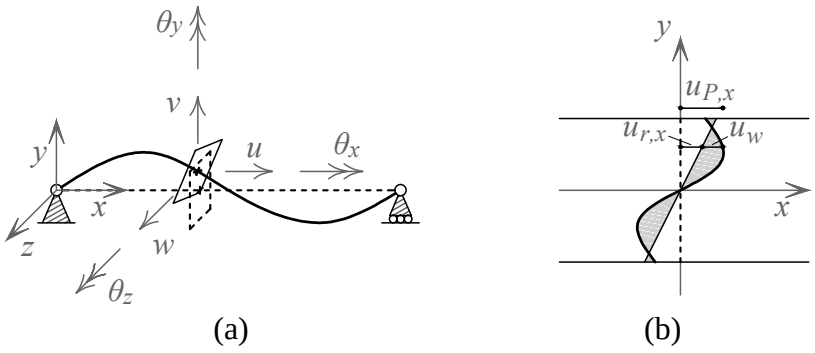

Figure 3: Cross-section rigid (a) and warping (b) displacements.

To describe the warping of the cross-section, the assumption of a rigid cross section is partially removed, by accounting for the out-of-plane deformations of the cross section, which still remains rigid in its plane. Hence, the displacement $\mathbf{u}_P(x, y, z)$ at the generic point P is expressed as the composition of the rigid part $\mathbf{u}_r(x, y, z) = \mathbf{a}_s(y, z) \, \mathbf{u}_s(x)$ and the displacement

$\mathbf{u}_w(x,y,z)$ due to the warping (Figure 3(b)):

$$\mathbf{u}_P(x,y,z) = \left\{ \begin{array}{c} u_{P,x}(x,y,z) \\ u_{P,y}(x,y,z) \\ u_{P,z}(x,y,z) \end{array} \right\} = \mathbf{a}_s(y,z)\,\mathbf{u}_s(x) + \mathbf{u}_w(x,y,z) \tag{8}$$

where $\mathbf{a}_s(y,z)$ is the compatibility operator, defined as:

$$\mathbf{a}_s(y,z) = \left[\begin{array}{cccccc} 1 & -y & 0 & 0 & z & 0 \\ 0 & 0 & 1 & -z & 0 & 0 \\ 0 & 0 & 0 & y & 0 & 1 \end{array} \right] \tag{9}$$

By applying the same operator, the strain vector is also evaluated as the sum of the rigid part $\boldsymbol{\epsilon}_r(x,y,z) = \mathbf{a}_s(y,z)\,\mathbf{e}(x)$ and that associated to the warping $\boldsymbol{\epsilon}_w(x,y,z)$:

$$\boldsymbol{\epsilon}(x,y,z) = \left\{ \begin{array}{c} \epsilon_x(x,y,z) \\ \gamma_{xy}(x,y,z) \\ \gamma_{xz}(x,y,z) \end{array} \right\} = \mathbf{a}_s(y,z)\,\mathbf{e}(x) + \boldsymbol{\epsilon}_w(x,y,z) \tag{10}$$

The generalized section deformation vector $\mathbf{e}(x)$ is:

$$\mathbf{e}(x) = \left\{ \begin{array}{c} \epsilon_G(x) \\ \chi_z(x) \\ \gamma_y(x) \\ \chi_x(x) \\ \chi_y(x) \\ \gamma_z(x) \end{array} \right\} = \left\{ \begin{array}{l} u'(x) \\ \theta'_z(x) \\ v'(x) - \theta_z(x) \\ \theta'_x(x) \\ \theta'_y(x) \\ w'(x) + \theta_y(x) \end{array} \right\} \tag{11}$$

where $\epsilon_G(x)$ is the axial strain, $\chi_z(x)$ and $\chi_y(x)$ are the curvatures, $\chi_x(x)$ the torsion rate of twist, and $\gamma_y(x)$ and $\gamma_z(x)$ the shear strains. As a consequence of the assumption that the section remains rigid in its plane, the warping displacement field has non-zero values only in the x direction, i.e.

$$\mathbf{u}_w(x,y,z) = \left\{ u_w(x,y,z) \quad 0 \quad 0 \right\}^T$$

Hence, the vector $\boldsymbol{\epsilon}_w(x,y,z)$ of the strains due to the warping displacements $u_w(x,y,z)$ becomes:

$$\boldsymbol{\epsilon}_w(x,y,z) = \left\{ \begin{array}{ccc} \frac{\partial u_w(x,y,z)}{\partial x} & \frac{\partial u_w(x,y,z)}{\partial y} & \frac{\partial u_w(x,y,z)}{\partial z} \end{array} \right\}^T \tag{12}$$

The stress components that are work conjugate with the strain quantities in $\boldsymbol{\epsilon}(x,y,z)$ are collected in the stress vector $\boldsymbol{\sigma}(x,y,z) = \left\{ \sigma_x(x,y,z) \quad \tau_{xy}(x,y,z) \quad \tau_{xz}(x,y,z) \right\}^T$, where σ_x is the normal stress along the beam axis direction, and τ_{xy} and τ_{xz} are the shear stresses in the plane of the cross-section parallel to the y and z–axis, respectively. With the virtual work equivalence the generalized stress vector $\mathbf{s}(x)$ is:

$$\mathbf{s}(x) = \int_A \mathbf{a}_s^T(y,z)\,\boldsymbol{\sigma}(x,y,z)\,dA = \left\{ \begin{array}{c} N(x) \\ M_z(x) \\ T_y(x) \\ M_x(x) \\ M_y(x) \\ T_z(x) \end{array} \right\} \tag{13}$$

where A is the cross-section area, $N(x)$ the axial stress, $M_z(x)$ and $M_y(x)$ are the bending moments, $M_x(x)$ the torsional moment, and $T_y(x)$ and $T_z(x)$ the generalized shear stresses.

From the element equilibrium in the undeformed configuration the stress vector $\mathbf{s}(x)$ can be expressed in terms the basic element force vector $\mathbf{q}$:

$$\mathbf{s}(x) = \mathbf{b}(x)\,\mathbf{q} + \mathbf{s}_p(x) \quad , \quad \mathbf{b}(x) = \begin{bmatrix} 1 & 0 & 0 & 0 & 0 & 0 \\ 0 & \frac{x}{L}-1 & \frac{x}{L} & 0 & 0 & 0 \\ 0 & -\frac{1}{L} & -\frac{1}{L} & 0 & 0 & 0 \\ 0 & 0 & 0 & 1 & 0 & 0 \\ 0 & 0 & 0 & 0 & \frac{x}{L}-1 & \frac{x}{L} \\ 0 & 0 & 0 & 0 & \frac{1}{L} & \frac{1}{L} \end{bmatrix} \tag{14}$$

where $\mathbf{b}(x)$ is the equilibrium matrix and $\mathbf{s}_p(x)$ the generalized section stresses under element loading. In addition to these forces, the force field $p_w(x, y, z)$ is work conjugate with the warping displacement $u_w(x, y, z)$ and arises at cross-sections with constrained warping displacements. In the element formulation in [12] the warping displacements u_w are treated as internal DOFs that are condensed out during the element state determination, as described in the next section. Consequently, only the standard twelve DOFs in (1) are associated with the global DOFs of the structural model.

2.1 Warping displacement interpolation

The study in [12] interpolates the warping displacement field $u_w(x, y, z)$ along the element axis x independently from the interpolation over the cross-section. The Gauss-Lobatto integration rule is used along the element axis using n_w points and 1D Lagrange polynomials $\mathrm{N}_i(x)$. At each Gauss-Lobatto point x_i, the warping displacements are interpolated over the cross-section by subdividing it into several rectangular patches with a regular distribution of interpolation points in each, for a total of s_w points (Figure 4). This approach defines a set of m_w 2D interpolation functions $\mathrm{M}_j(y, z)$ for the warping DOFs.

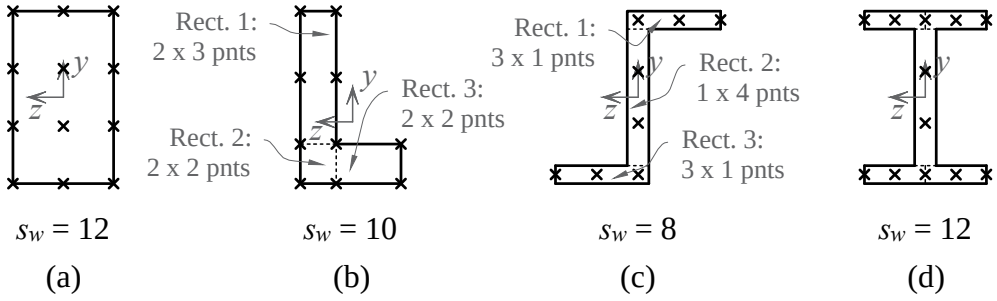

Figure 4: Warping interpolation points over the element cross-section.

This study explores the use of Hermite polynomials for the warping displacements in addition to the Lagrange polynomials used in [12]. For the Lagrange polynomials only one internal DOF is required at each integration point of the warping displacement u_w (Figure 5(a)) and the total number m_w of warping DOFs is equal to the number s_w of integration points. In contrast, Hermite polynomials required three internal DOFs at each integration point, one for the warping displacement u_w, and two for the derivatives $\partial u_w/\partial y$ and $\partial u_w/\partial z$ (Figure 5(b)). In this

case the total number m_w of warping DOFs is equal to three times the number s_w of integration points, $m_w = 3\,s_w$.

Henceforth, $u_{w,ij}$ denotes the generic j-th warping DOF at section x_i, coinciding with the displacements u_w for Lagrange polynomials, and with the displacements u_w and their derivatives for Hermite polynomials:

$$\begin{aligned} \{u_{w,1}, \quad u_{w,2}, \quad u_{w,3}, \ldots\} &= \{u_w^{pnt\,1}, \quad u_w^{pnt\,2}, \quad u_w^{pnt\,3}, \ldots\} \quad Lagrange \\ \{u_{w,1}, \quad u_{w,2}, \quad u_{w,3}, \ldots\} &= \{u_w^{pnt\,1}, \quad \tfrac{\partial u_w^{pnt\,1}}{\partial y}, \quad \tfrac{\partial u_w^{pnt\,1}}{\partial z}, \ldots\} \quad Hermite \end{aligned} \tag{15}$$

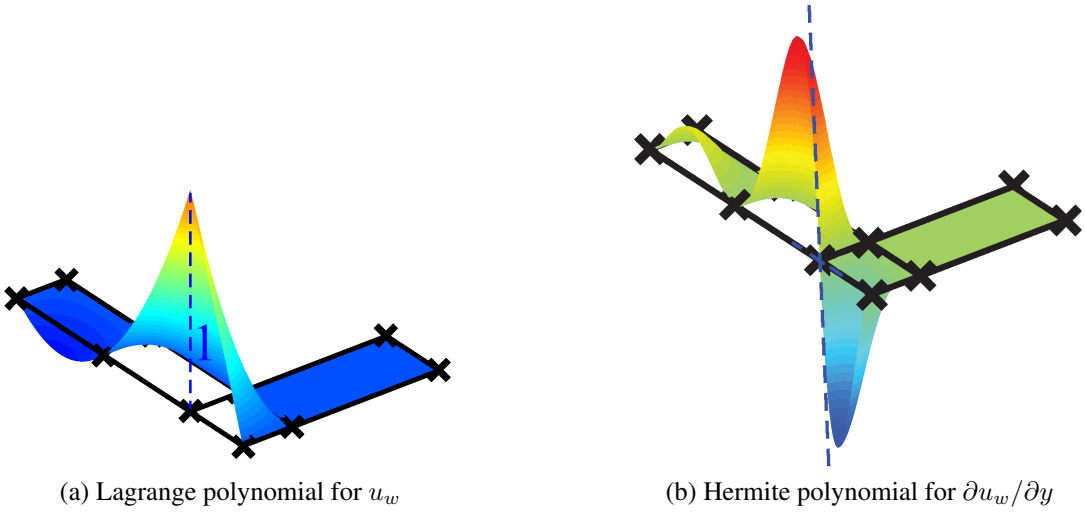

(a) Lagrange polynomial for u_w (b) Hermite polynomial for $\partial u_w/\partial y$

Figure 5: Example of polynomial interpolation function in a cross-section composed by a set of rectangular portions: L-shaped section of Figure 4(b), $m_w = 10$ for Lagrange and $m_w = 30$ for Hermite.

The interpolation of the warping displacement field $u_w(x, y, z)$ thus is:

$$u_w(x, y, z) = \sum_{i=1}^{n_w} \mathrm{N}_i(x)\, u_{w,i}(x_i, y, z) = \sum_{i=1}^{n_w} \mathrm{N}_i(x)\, \mathbf{M}(y, z)\, \mathbf{u}_{w,i} \tag{16}$$

with the following expression for the interpolation of $u_{w,i}(x_i, y, z)$ at section i:

$$u_{w,i}(x_i, y, z) = \sum_{j=1}^{m_w} \mathrm{M}_j(y, z)\, u_{w,ij} = \mathbf{M}(y, z)\, \mathbf{u}_{w,i} \tag{17}$$

$\mathbf{u}_{w,i}$ is a column vector with all m_w warping DOFs $u_{w,ij}$ at section i (following the order in Equation (15)) and $\mathbf{M}(y, z)$ is a row vector with all m_w shape functions $M_j(y, z)$ defined over the cross-section.

It is important to point out the following difference between Lagrange and Hermite polynomials. Because for the Lagrange polynomials all warping DOFs correspond to warping displacement values the condition of warping restraint $u_{w,ij} = 0$ can be applied to each polynomial separately, so that even a single point or a specific portion of the cross-section can be restrained. In contrast, for the Hermite polynomials some of the warping DOFs are the derivatives of the warping displacement field in the cross-section. This requires the restraint of all displacements of the particular cross-section at the same time, thus ensuring that $u_w = \partial u_w/\partial y = \partial u_w/\partial z = 0$ is satisfied on the cross-section.

The vector $\mathbf{p}_{w,i}$ collecting the warping forces $p_{w,i}$ at the points located on the i-th section can be defined, which is work conjugated with $\mathbf{u}_{w,i}$.

2.2 Element variational formulation

This section describes the main aspects of the element formulation and focuses on the role played by the warping DOFs in the governing equations.

The equations governing the element state determination are derived on the basis of a modified Hu-Wahizu variational principle, depending on the four independent fields $\mathbf{u}_s(x)$, $\mathbf{e}(x)$, $\boldsymbol{\sigma}(x,y,z)$ and $u_w(x,y,z)$ [12]:

$$\Pi(\mathbf{u}_s, \mathbf{e}, \boldsymbol{\sigma}, u_w) = \int_V \boldsymbol{\sigma}^T \mathbf{a}_s \left[\mathbf{e}(\mathbf{u}_s) - \mathbf{e}\right] dV + \int_V W(\mathbf{e}, \boldsymbol{\epsilon}_w)\, dV - \mathbf{u}^T \mathbf{p} - \int_0^L \mathbf{u}_s^T \mathbf{p}_s\, dx \quad (18)$$

where $W(\mathbf{e}, \boldsymbol{\epsilon}_w)$ is the internal potential energy and $\mathbf{p}_s$ denotes the loads along the element axis. The stationarity of Π with respect to the four independent fields gives the following governing equations:

Stationarity with respect to:	Governing equation:	
$\mathbf{u}_s(x)$	$\mathbf{a}_g^T \mathbf{q} = \mathbf{p} + \mathbf{p}_{rp}$	(19a)
$\mathbf{e}(x)$	$\boldsymbol{\sigma}(x,y,z) = \hat{\boldsymbol{\sigma}}[\boldsymbol{\epsilon}(x,y,z)]$	(19b)
$\boldsymbol{\sigma}(x,y,z)$	$\mathbf{v} = \int_0^L \mathbf{b}^T(x)\, \mathbf{e}(x)\, dx$	(19c)
$u_w(x,y,z)$	$\mathbf{p}_{w,i} = \int_0^L \frac{\partial \mathrm{N}_i}{\partial x} \mathbf{s}_w^x\, dx + \int_0^L \mathrm{N}_i\, \mathbf{s}_w^{yz}\, dx$	(19d)

The first three (19a), (19b) and (19c) are the equations of the standard three-field mixed formulation [4], and govern the element equilibrium, the material constitutive law and the element compatibility, respectively. The vector $\mathbf{p}_{rp}$ collects the nodal forces under element loading. Equation (19d), represents the section equilibrium equation under warping displacements. The stresses $\mathbf{s}_w^x$ and $\mathbf{s}_w^{yz}$ are the generalized stresses due to section warping, as defined by the integral of the material stresses $\boldsymbol{\sigma}(x,y,z)$ over the cross-section:

$$\mathbf{s}_w(x) = \left\{ \begin{array}{c} \mathbf{s}_w^x(x) \\ \mathbf{s}_w^{yz}(x) \end{array} \right\} = \left\{ \begin{array}{c} \int_A \left[\mathbf{a}_w^x(y,z)\right]^T \boldsymbol{\sigma}(x,y,z)\, dA \\ \int_A \left[\mathbf{a}_w^{yz}(y,z)\right]^T \boldsymbol{\sigma}(x,y,z)\, dA \end{array} \right\} \quad (20)$$

with $\mathbf{a}_w^x(y,z)$, $\mathbf{a}_w^{yz}(y,z)$ being $3 \times m_w$ matrices of the following form:

$$\mathbf{a}_w^x(y,z) = \left[\begin{array}{c} \mathbf{M}(y,z) \\ \mathbf{0} \\ \mathbf{0} \end{array} \right] \quad , \quad \mathbf{a}_w^{yz}(y,z) = \left[\begin{array}{c} \mathbf{0} \\ \frac{\partial \mathbf{M}(y,z)}{\partial y} \\ \frac{\partial \mathbf{M}(y,z)}{\partial z} \end{array} \right] \quad (21)$$

The nonlinear system of equations (19) are solved by iteration of their linearized form [12].

3 CORRELATION STUDIES

This section discusses the correlation study of two specimens for validating the 3d beam formulation. The Matlab toolbox FEDEASLab [16] is used for investigating the capability of the

model to represent the damage evolution of frame members when relevant warping deformations arise. To this end, two different prismatic beams under end torsional loads are considered, from the experimental tests of plain concrete specimens by [17] and of RC specimens by [18]. In this framework, advantages and disadvantages of the use of Hermite polynomials vs. Lagrange polynomials for the warping interpolation functions are discussed.

The Gauss-Lobatto integration rule is adopted for the integrals along the element axis together with a fiber discretization of the cross-section using the mid-point rule [6]. The nonlinear material relation of the following section is used for each concrete fiber and the classical J2 plasticity model is used for the steel bars.

3.1 Damage model

In this study the constitutive behavior of concrete is described with the damage material model in [15]. The model uses a scalar damage variable D to define the relation between the strain tensor $\mathbf{E}$ and the stress tensor $\mathbf{\Sigma}$:

$$\mathbf{E} = \frac{(1+\nu)\mathbf{\Sigma} - \nu\,\mathrm{tr}(\mathbf{\Sigma})\,\mathbf{I}}{E(1-D)} \tag{22}$$

where E in the material Young modulus and ν the Poisson ratio, and $\mathbf{I}$ is the second order identity tensor. The damage variable D, bounded in the range $[0 \quad 1]$, where $D = 0$ correponds to initial undamaged state and $D = 1$ to the complete degraded state, is a function of a single variable Y, which is the combination of two strain measures Y_t and Y_c for cracking (tensile state) and crushing (compressive state), respectively. The combination gives:

$$Y = r\,Y_t + (1-r)\;Y_c \qquad \text{with} \quad r = \frac{\sum \left\langle \hat{\bar{\sigma}}_i \right\rangle_+}{\sum |\hat{\bar{\sigma}}_i|} \in [0;1] \tag{23}$$

where $\hat{\bar{\sigma}}_i$ are the principal effective stresses.

The evolution law for D is defined by the following exponential relation:

$$D = 1 - \frac{Y_0(1-A)}{Y} - A\,e^{-B(Y-Y_0)} \tag{24}$$

where $Y_0 = r\,\epsilon_{0,t} + (1-r)\;\epsilon_{0,c}$ is the initial threshold for Y and A and B are material parameters, also defined from the combination of the tensile and compressive parameters, $A_{t/c}$ and $B_{t/c}$, respectively according to:

$$A = A_t\left(2\,r^2\,(1-2k) - r\,(1-4k)\right) + A_c\left(2\,r^2 - 3\,r + 1\right) \tag{25}$$

$$B = r^q B_t + (1-r^q)\,B_c \qquad \text{with} \quad q = r^2 - 2r + 2 \tag{26}$$

k is a parameter for calibrating the asymptotic stress value at large shear deformations and is set equal to 0.7 throughout the following simulations.

Figure 6(a) and 6(b) shows the resulting stress-strain constitutive relation and the damage evolution law with the material parameters in the first row of Table 1.

3.2 Plain concrete and RC beams subjected to end torsional loads

Two prismatic beams under pure torsion are used for the validation of the 3d beam formulation. Both specimens have a total length of 160 cm, and are divided into three parts: two end

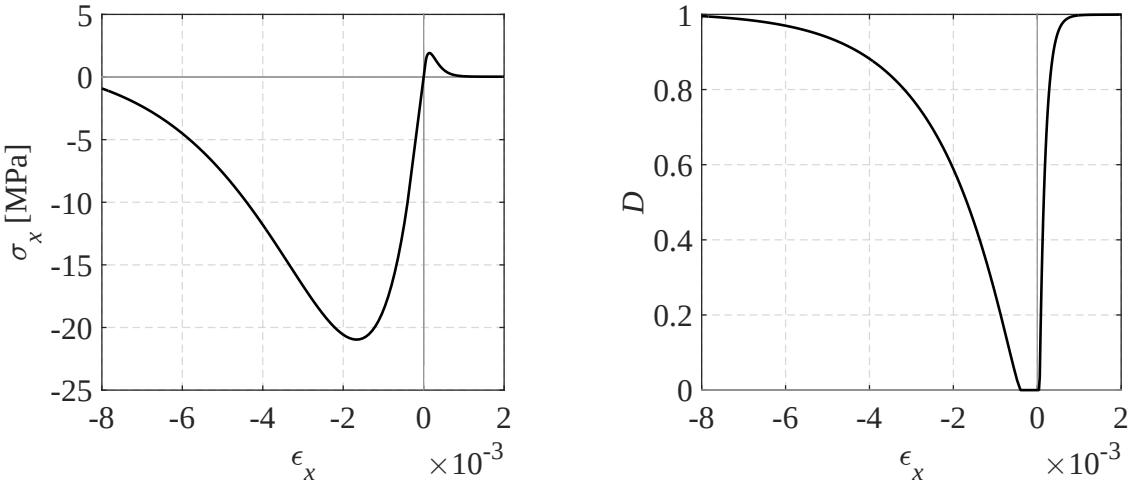

(a) Uniaxial stress-strain relation. (b) Damage evolution law.

Figure 6: Damage constitutive law for concrete.

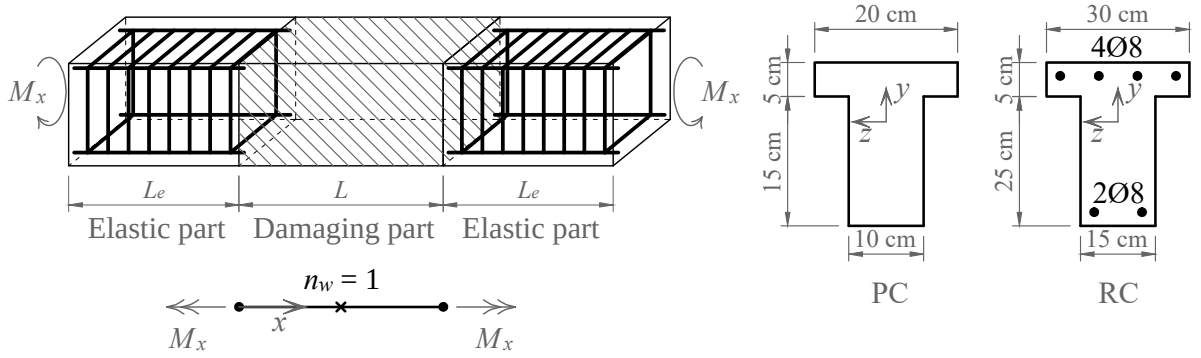

Figure 7: Beams subjected to end torsional loads: specimens geometry.

regions of length L_e, reinforced so as to remain elastic, and a middle part of length L undergoing cracking and damage (Figure 7). For pure torsion a torsional moment M_x is applied at both ends with a particular arrangement that allows the beam cross-sections to undergo warping.

The plain concrete (PC) and the reinforced concrete (RC) cross-section in Figure 7 are considered for the central damaging part of the beam. The geometrical parameters are: $L = 60$ cm for the former one ($L_e = 50$ cm) and $L = 100$ cm for the latter one ($L_e = 30$ cm). Only the middle part is modeled in the numerical analysis, using one FE with one warping interpolation point located along the axis, $n_w = 1$ (Figure 7), as a uniform warping distribution is expected in this direction. Three Gauss-Lobatto quadrature points are used for the integration along the FE with a uniform fiber discretization made of 86 fibers at each point. The material parameters are given in Table 1. Modulus E is not specified in the two reference papers, thus it is adjusted to reproduce the measured initial stiffness. For the steel bars, which are modeled as additional fibers, the following material parameters are used: Young modulus $E = 210000\,\mathrm{MPa}$, Poisson coefficient $\nu = 0.3$, yield stress $f_y = 560\,\mathrm{MPa}$, isotropic hardening $H_i = 0.001\,E$ and kinematic hardening $H_k = 0.01\,E$.

Four different warping DOFs distributions in Figure 8 are considered. The first two adopt Lagrange polynomials, L1(12) and L2(30) and the other two use Hermite polynomials, H1(12) and H2(30) with the total number of internal DOFs in parentheses.

	E [MPa]	ν	$\varepsilon_{0,t}$	A_t	B_t	$\varepsilon_{0,c}$	A_c	B_c
PC	25 000	0.20	0.000055	0.98	7 000	0.000200	1.30	600
RC	30 000	0.20	0.000100	0.98	11 000	0.000200	1.50	600

Table 1: Beams subjected to end torsional loads: material parameters for concrete.

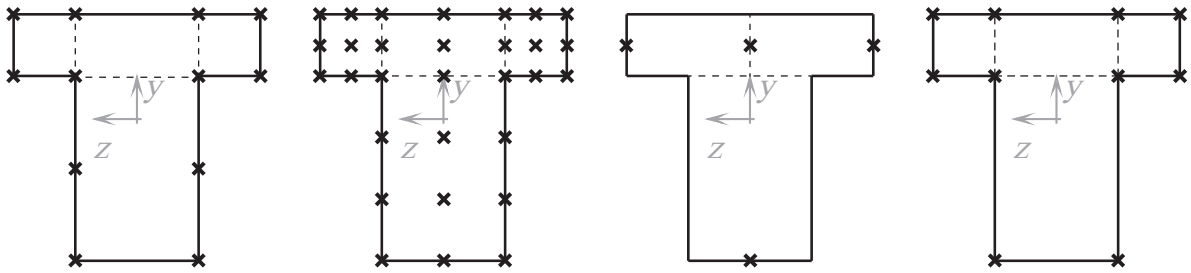

(a) L1(12) (b) L2(30) (c) H1(12) (d) H2(30)

Figure 8: Warping DOFs distribution over the cross-section of the T-shaped beams ("L" = Lagrange interpolation functions, "H" = Hermite interpolation functions and the number in the parentheses indicates the total number m_w of warping DOFs).

Figure 9(a) compares the global response for the four warping distributions with the experimental results for the plain concrete beam. The H2(30) model gives the best solution, since it adopts cubic interpolation functions in the y and z direction. The L2(30) model uses the same number of warping DOFs and, although it provides parabolic interpolation functions (cubic only in the y direction for the web), it gives a solution that agrees very well with the solution of the H2(30) model. The L1(12) model with linear interpolation functions, slightly overestimates the element strength, with a significantly smaller number of warping DOFs. Finally, the H1(12) model, which uses the same number of warping DOFs with linear interpolation functions as the L1(12) model, underestimates both the stiffness and the strength of the element. These results lead to the conclusion that Lagrange polynomials are a good compromise between accuracy and computational efficiency. In fact, with a small number of warping DOFs these interpolation functions give satisfactory solutions, whereas for the Hermite polynomials high order interpolation polynomials are required over the cross section. For sections composed of thin rectangular segments, as is the case for the commercial steel profiles, linear Lagrange polynomial prove computationally superior (see [12]) to the Hermite polynomials which require many warping DOFs for good results.

Figure 9(b) compares the results of the H2(30) model with the experimental results in [17] and with the analytical results of the same study under the assumption of a rigid cross-section. The response under the assumption of a rigid cross-section results from a value of $J = 6\,774\,\mathrm{cm}^4$ for the polar moment of area based on the semi-analytical solution with Fourier series.

Figure 9(b) shows that the rigid section assumption overestimates the peak load, since the damage distribution over the cross-section is not captured correctly. In fact, Figure 10 shows that the distribution of damage variable D is similar to that for a circular section where warping is not possible. Instead, in the presence of warping the damage distribution is much more diffused over the whole cross-section. Figure 11 shows the γ_{xy} distribution. Note that the section warping gives rise to parabolic distributions of the shear strains γ_{xy} and γ_{xz} over the section. In contrast, the rigid section assumption is associated with in a linear distribution of

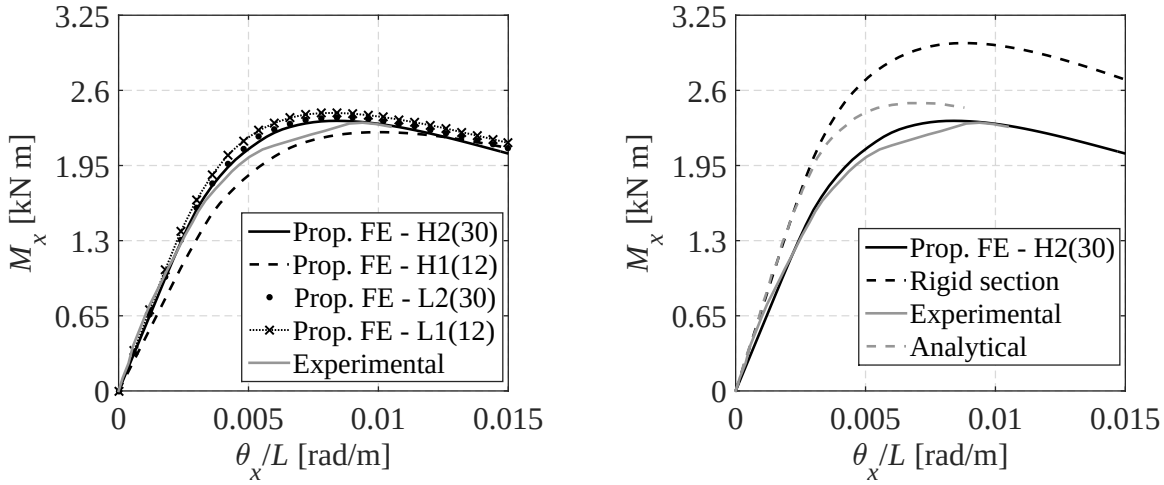

(a) Comparison between the different warping distributions.

(b) Numerical vs experimental response.

Figure 9: Response of the T-shaped plain concrete beam: moment vs rotation per unit length.

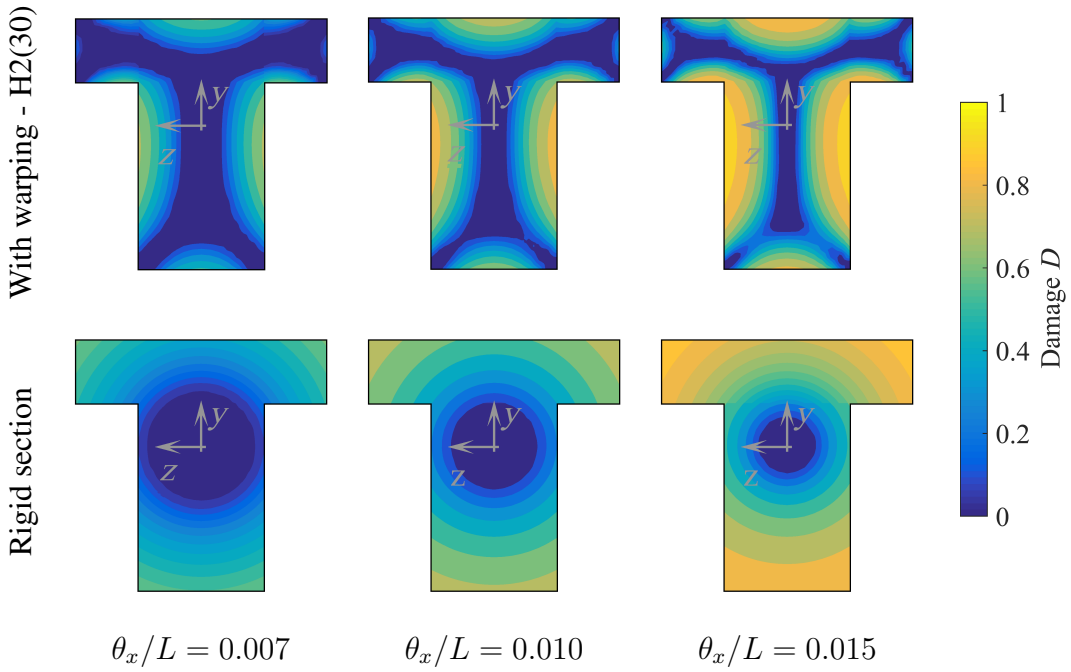

Figure 10: Evolution of the damage over the plain concrete T-shaped cross-section with and without warping.

these strains in the y and z direction.

Similar observations result for the RC beam whose global response is shown in Figure 12. The response under the assumption of a rigid cross-section results from a value of $J = 32\,642\,\mathrm{cm}^4$ for the polar moment of area based on the semi-analytical solution with Fourier series. The response of the plain concrete beam with the H2(30) model is superimposed on the same figure for contrast. The comparison shows that the reinforcing bars increase the member strength slightly under high values of torsional deformation, when the concrete is completely damaged. The experimental response shows greater strength under intermediate deformations, as the beam transitions from the uncracked to the fully cracked state, but this transitory behavior

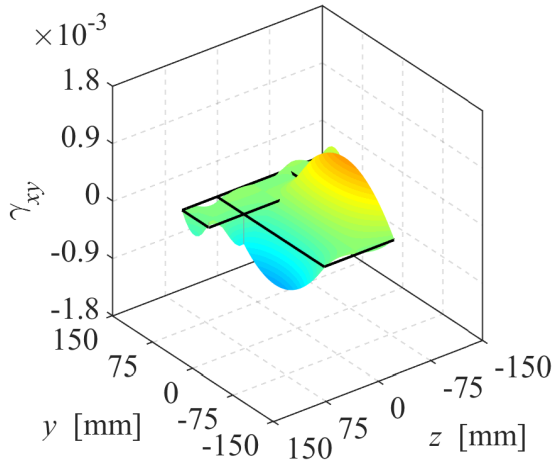

Figure 11: Shear strain in the plain concrete section - Model with warping, H2(30) - $\theta_x/L = 0.007$.

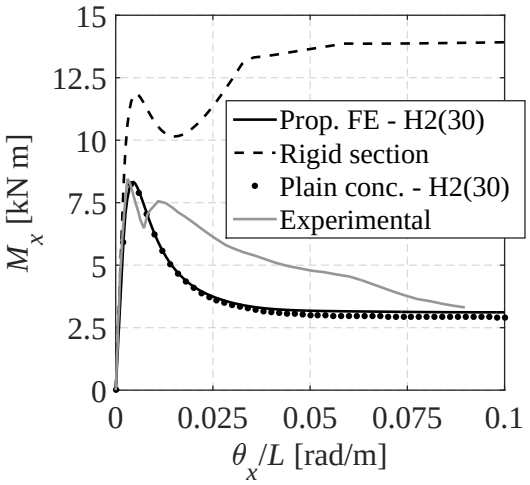

Figure 12: Numerical vs experimental response for the RC beam: moment vs rotation per unit length.

due to rough cracks and dowel action is not accounted for in the present numerical model.

4 CONCLUSIONS

- The paper extends an existing 3d enhanced fiber beam element formulation with warping degrees of freedom to the analysis of concrete beams under torsion with warping by incorporating a constitutive material law with damage.
- Two examples demonstrate the capabilities of the element for describing the inelastic response of plain concrete and RC members under torque, as well as the resulting shear strain-stress and damage distributions over the cross-section.
- The numerical analyses show the importance of the interaction between the warping deformations and the damage progression. In fact, the standard elements, that account for the torsional effects in a simplified way, give unrealistic results and overestimate both the strength and the ductility of the structure.
- The 3d enhanced fiber beam element proves to be robust and accurate and has significantly lower computational cost than shell and brick finite elements, while delivering results of excellent accuracy for the local response of the structural members.

REFERENCES

[1] V. Ciampi, L. Carlesimo .A nonlinear beam element for seismic analysis of structures, *Proceedings of the Eighth European Conference on Earthquake Engeneering*, Laboratorio Nacional de Engenharia, Lisbon, 1986.

[2] A. Neuenhofer, F.C. Filippou. Evalutation of nonlinear frame finite-element models, *Journal of Structural Engineering*, **123**, 958–966, 1997.

[3] D. Addessi, V. Ciampi. A regularized force-based beam element with a damage-plastic section constitutive law, *International Journal for Numerical Methods in Engineering*, **70**, 610–629, 2007.

[4] A. Saritas, O. Soydas. Variational base and solution strategies for non-linear force-based beam finite elements, *International Journal of Non-Linear Mechanics*, **47**, 54–64, 2012.

[5] M.H. Scott, G.L. Fenves. Plastic hinge integration methods for force-based beam-column elements, *Journal of Structural Engineering*, **132**, 244-252, 2006.

[6] S.M. Kostic, F.C. Filippou. Section discretization of fiber beam-column elements for cyclic inelastic response, *Journal of Structural Engineering*, **138**, 592–601, 2012.

[7] J. M. Bairan Garcia, A. R. Mari Bernat. Coupled model for the non-linear analysis of anisotropic sections subjected to general 3D loading. Part 1: Theoretical formulation, *Computers and Structures*, **84**, 2254–2263, 2006.

[8] J. N. Gregori, P. M. Sosa, M.A. F. Prada, F. C. Filippou. A 3D numerical model for reinforced and prestressed concrete elements subjected to combined axial, bending, shear and torsion loading. *Engineering Structures*, **29**, 3404–3419, 2007.

[9] A. Saritas, F.C. Filippou. Inelastic axial-flexure shear coupling in a mixed formulation beam finite element, *International Journal of Nonlinear Mechanics*, **44**, 913-922, 2009.

[10] S. Mohr, J. M. Bairan Garcia, A. R. Mari Bernat. A frame element model for the analysis of reinforced concrete structures under shear and bending, *Engineering Structures*, **32**, 3936–3954, 2010.

[11] S. Zhou. Finite beam element considering shear-lag effect in box girder, *Journal of Engineering Mechanics*, **136**, 11151122, 2010.

[12] V. Le Corvec. Nonlinear 3d frame element with multi-axial coupling under consideration of local effects, *UC Berkeley Electronic Theses and Dissertations Degree: Ph.D.*, Civil and Environmental Engineering, UC Berkeley, 2012.

[13] V. Le Corvec, F.C. Filippou. Enhanced 3D Fiber beam-column element with warping displacements. *Proceedings 3rd International Conference on Computational Methods in Structural Dynamics and Earthquake Engineering COMPDYN, ECCOMAS*, Corfu, Greece, 2011.

[14] D. Addessi, P. Di Re. A 3D mixed frame element with multi-axial coupling for thin-walled structures with damage, *Frattura ed Integrità Strutturale*, **29**, 178-195, 2014.

[15] J. Mazars, F. Hamon, S. Grange. A new 3D damage model for concrete under monotonic, cyclic and dynamic loadings, *Materials and Structures*, DOI 10.1617/s11527-014-0439-8, 2014.

[16] F. C. Filippou, M. Constantinides. Fedeaslab getting started guide and simulation examples, *Technical Report 22, NEESgrid*, www.nees-grid.org, 2004.

[17] C. J. Karayannis, C. E. Chalioris. Experimental validation of smeared analysis for plain concrete in torsion, *Journal of Structural Engineering*, **126**, 646–653, 2000.

[18] C. E. Chalioris. Torsional strengthening of rectangular and flanged beams using carbon fibre-reinforced-polymers Experimental study, *Construction and Building Materials*, **22**, 21–29, 2008.